SUPPORT INFORMATION for

A CO-mediated Photothermal Therapy to Kill Drug-resistant Bacteria and Minimize Thermal Injury for Infected Diabetic Wound Healing

Xin Jin,[1#] Zelin Ou,[2,3#] Guowei Zhang,[3#] Rong Shi,[3] Jumin Yang,[1] Wenguang Liu,[1] Gaoxing Luo[2,3], Jun Deng,[3*] Wei Wang[4,5*]*

[1]Tianjin Key Laboratory of Composite and Functional Materials, School of Materials Science and Engineering, Tianjin University, Tianjin 300350, China.

[2]Department of Nephrology, The First Affiliated Hospital of Wenzhou Medical University, Wenzhou 325035, China.

[3]Institute of Burn Research, State Key Lab of Trauma, Burn, and Combined Injury, Chongqing Key Laboratory for Disease Proteomics, Southwest Hospital, Third Military Medical University (Army Medical University), Chongqing 400038, China.

[4]ZJU-Hangzhou Global Scientific and Technological Innovation Center, Hangzhou, Zhejiang 311215, China.

[5]College of Chemical and Biological Engineering, Zhejiang University, Hangzhou 310027, China.

[#]These authors contributed equally to this work: Xin Jin, Zelin Ou, and Guowei Zhang.

*Corresponding authors: Gaoxing Luo, logxw@hotmail.com; Jun Deng, Email: djun.123@163.com; Wei Wang, Email: wwgfz@zju.edu.cn.

This PDF includes:

Supplemental methods

Table S1-S4

Fig. S1-S22

Supplemental methods

The calculation of photothermal conversion efficiency

To investigate photothermal conversion efficiency (η) of the materials, 500 μL of mPDA NPs or CO@mPDA NPs (500 μg mL^{-1}) were added into a 48-well plate. The well underwent an irradiation with laser power density of 1.8 W cm^{-2} for 10 mins and then a natural cooling for another 10 mins. The temperature was recorded by the IR camera (FLIR E40, US) every 30 s.

The photothermal conversion efficiency was calculated according to the following formulas (**Eq. 1-3**). Q_0 stands for the background energy input in water. T_{water}, T_{max}, and T_{surr} represent the maximum temperature of water (30.2 °C), materials suspension, and the environment (25.0 °C). I is the laser power (1.8 W). $A808$ represents the absorbance at 808 nm measured by ultraviolet spectrum (UV, UV-2600, Shimadzu, Japan). h and S are the heat transfer coefficient and surface area of the container, respectively, which are unknown in the system. τ_s is a time constant that can be determined by the slope linear regression from the cooling time vs-ln($\Delta T/\Delta T_{max}$) to calculate hS value, where ΔT and ΔT_{max} is the real time and maximum temperature change of the liquid, and m and C are the liquid mass (500 mg) and heat capacity (4.2 J g^{-1} K^{-1}), respectively.

$$\eta = \frac{hS(T_{max} - T_{surr}) - Q_0}{I(1 - 10^{-A808})} \qquad \textbf{Eq. 1}$$

$$Q_0 = hS(T_{water} - T_{surr}) \qquad \textbf{Eq. 2}$$

$$\tau_s = \frac{mC}{hS} \qquad \textbf{Eq. 3}$$

Supplemental Tables and Figures

Table S1. Sequences of the primers used for RT-qPCR

Gene	Forward sequences (5'→3')	Reverse sequences (5'→3')
Hsp90	TGACTGTCATCACCAAGCATAATG	GTCACGTTCCTTCTCCACAAAGA
Hspa1	CACCTAAGGCTGAGACTCTTGTT	ACACAAGACCTGGCAAGTTCTTT
Hspa4	GAGGCGATGGAGTGGATGAATAG	ACTTTGGGTTTGGGCTTTGAAAT
Hspa9	GTGTGTTGGCTGGTGATGTTACA	TTTGTCCATCAGCAGCAGTAGAA
Ahsa1	ACAAGTCTCGTGGCCTTAATGAA	CATTCACTGTGGGCAAGATCATG
Dnak	GACGCCTGGGTGGAAGTGA	CGCTGGCTGTCGTTGAAGTAG

Table S2. Nonlinear regression parameters of Gompertz model in the four stages

	1St NIR on	1st NIR off	2nd NIR on	2nd NIR off
Y_M (μM mg^{-1})	6.667	2.781	0.671	0.539
Y_0 (μM mg^{-1})	< 0.001	0.132	< 0.001	0.057
K (min^{-1})	0.195	0.293	0.364	0.282
R^2	0.999	0.996	0.992	0.970

Table S3. Grouping for interaction term by two-way ANOVA

	mPDA	**mPDA+NIR**	**CO@mPDA**	**CO@mPDA+NIR**
Variable I (CO)	-	-	+	+
Variable II (NIR)	-	+	-	+

Table S4. Statistical results of interaction term by two-way ANOVA

Interaction term	*SS*	*DF*	*MS*	*DFn*	*DFd*	*F* (*DFn*, *DFd*)	*P*
Value	846.9	1	846.9	1	8	16.50	0.0036

Abbreviations: *SS* stood for sum of squares; *DF* stood for degrees of freedom; *MS* stood for mean square; *DFn* stood for degrees of freedom numerator; *DFd* stood for degrees of freedom denominator. *F* and *P* were statistical parameters for significance analysis of interaction term.

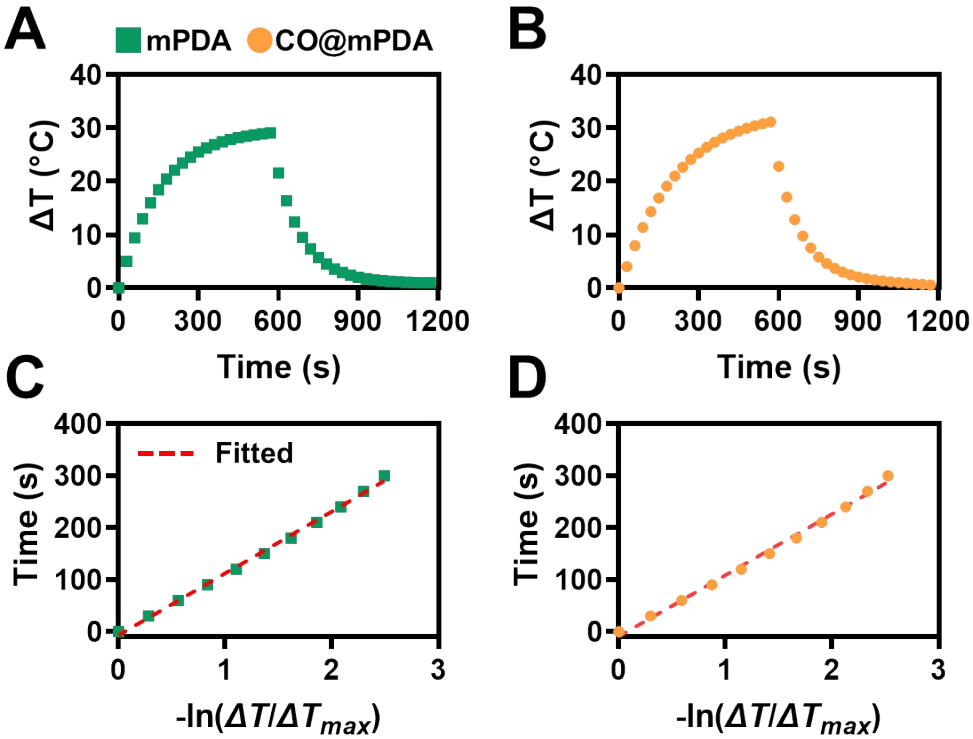

Fig. S1. investigation of photothermal conversion efficiency of the materials.

(A and B) The heating and cooling curves of mPDA (A) and CO@mPDA (B). (C and D) The linear regression of cooling time vs -ln($\Delta T/\Delta T_{max}$) with mPDA (C) and CO@mPDA (D).

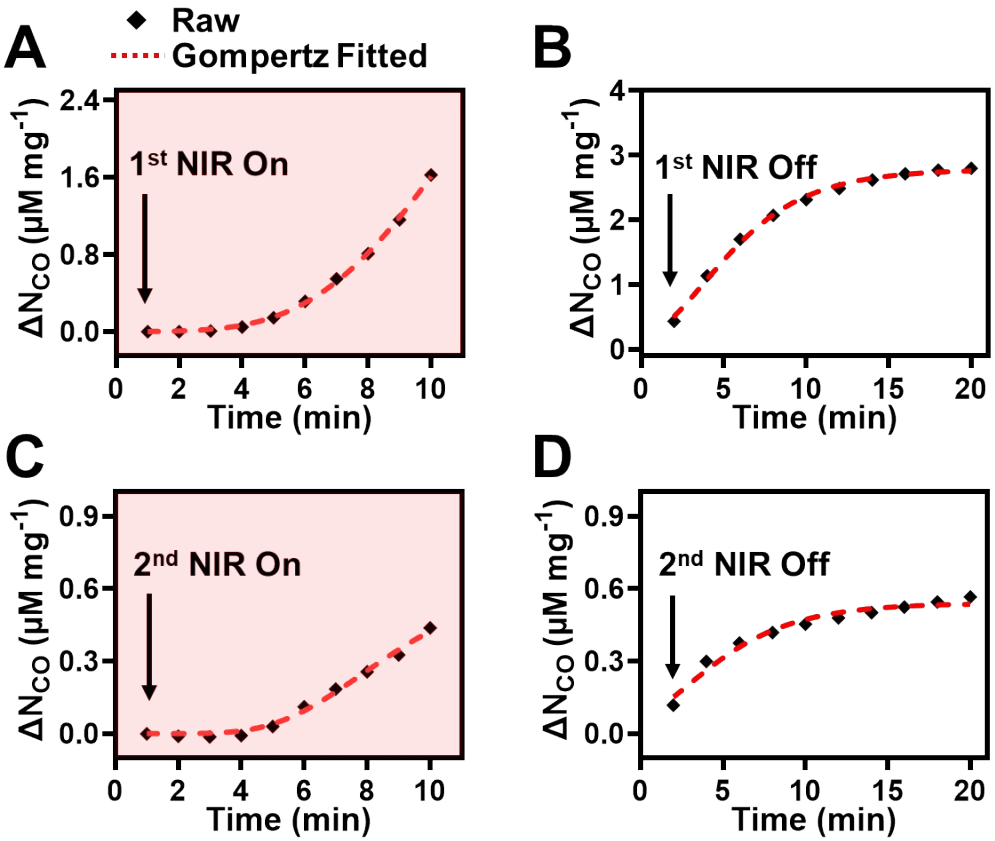

Fig. S2. Nonlinear regression of released CO amount by Gompertz function.

Gompertz fitted curve of released CO amount (n = 10 in each set of raw data) in the first round when NIR is on (A) or off (B), and the second round with NIR on (C) or off (D).

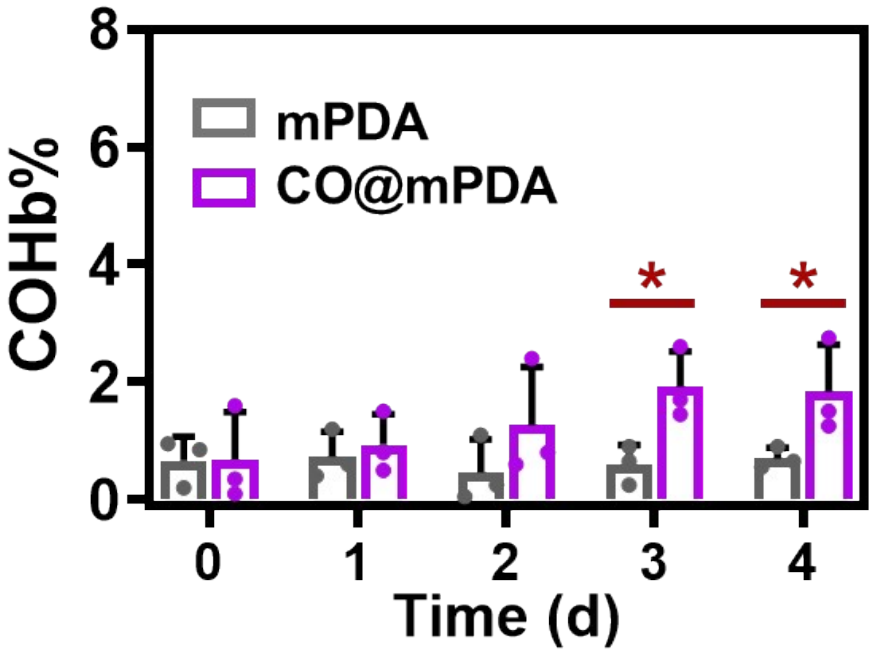

Fig. S3. CO release measured by a blood gas analyzer *in vitro*.

COHb% after co-incubation with rat blood and materials *in vitro*. All data are shown as mean ± s.d. (n = 3). The differences were determined by student's t-test between two groups. The significance was marked as '**' for $P < 0.01$, '*' for $P < 0.05$ and 'ns' for $P > 0.05$.

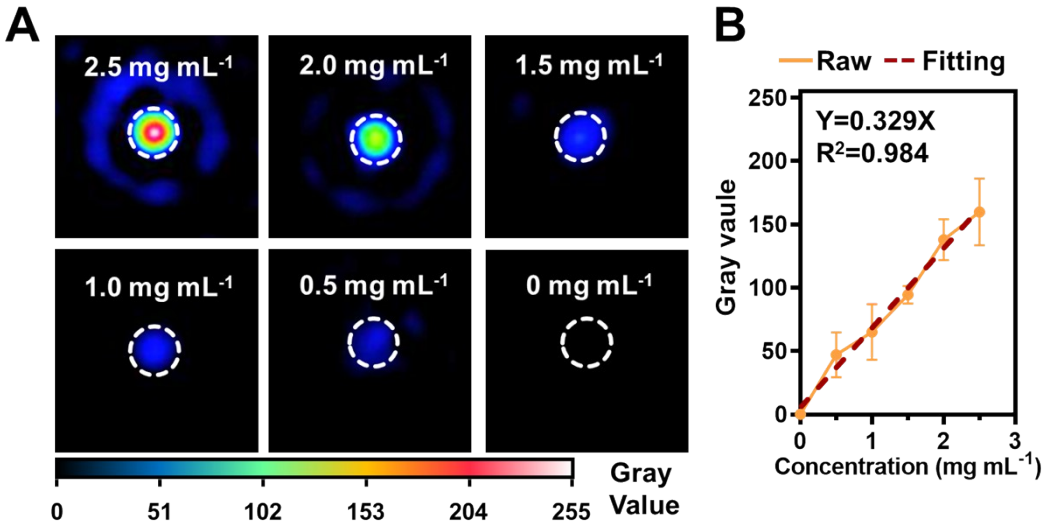

Fig. S4. Photoacoustic conversion performance of CO@mPDA.

(A) Photoacoustic signal of CO@mPDA with various concentrations. (B) Statistically quantitative result of photoacoustic signal. All data are shown as mean ± s.d. (n = 3).

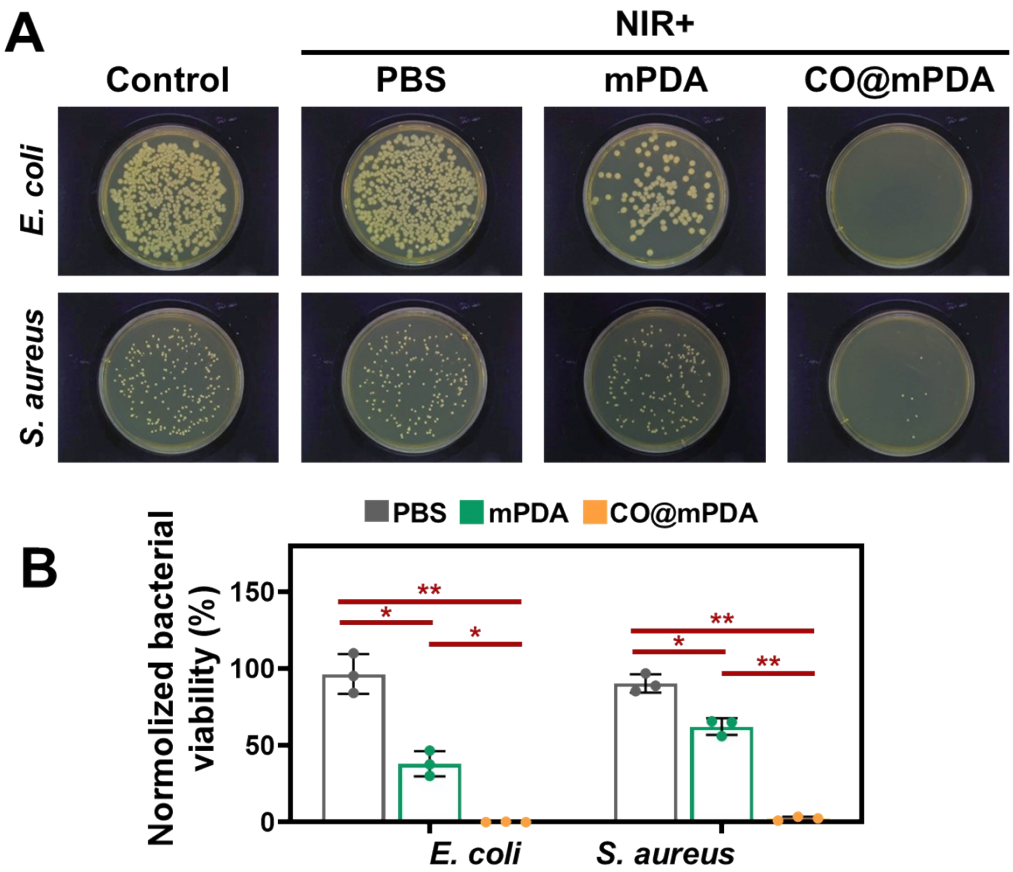

Fig. S5. *In-vitro* antibacterial performance for *E. coil* and *S. aureus*.

(A-B) Representative images of plate culture (A) and their statistical results (B) by various treatments. All data are shown as mean ± s.d. (n = 3). The differences were determined by one-way ANOVA. The significance was marked as '**' for $P < 0.01$, '*' for $P < 0.05$, and 'ns' for $P > 0.05$.

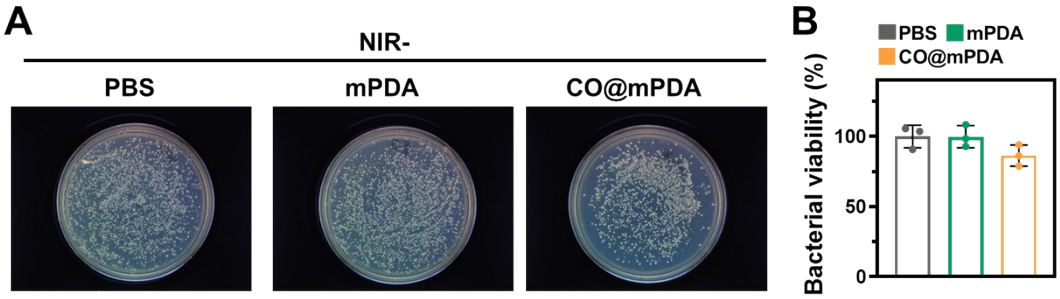

Fig. S6. *In-vitro* antibacterial performance of NPs without NIR for MRSA.

(A-B) Representative images of plate culture (A) and their statistical results (B) by various treatments without NIR.

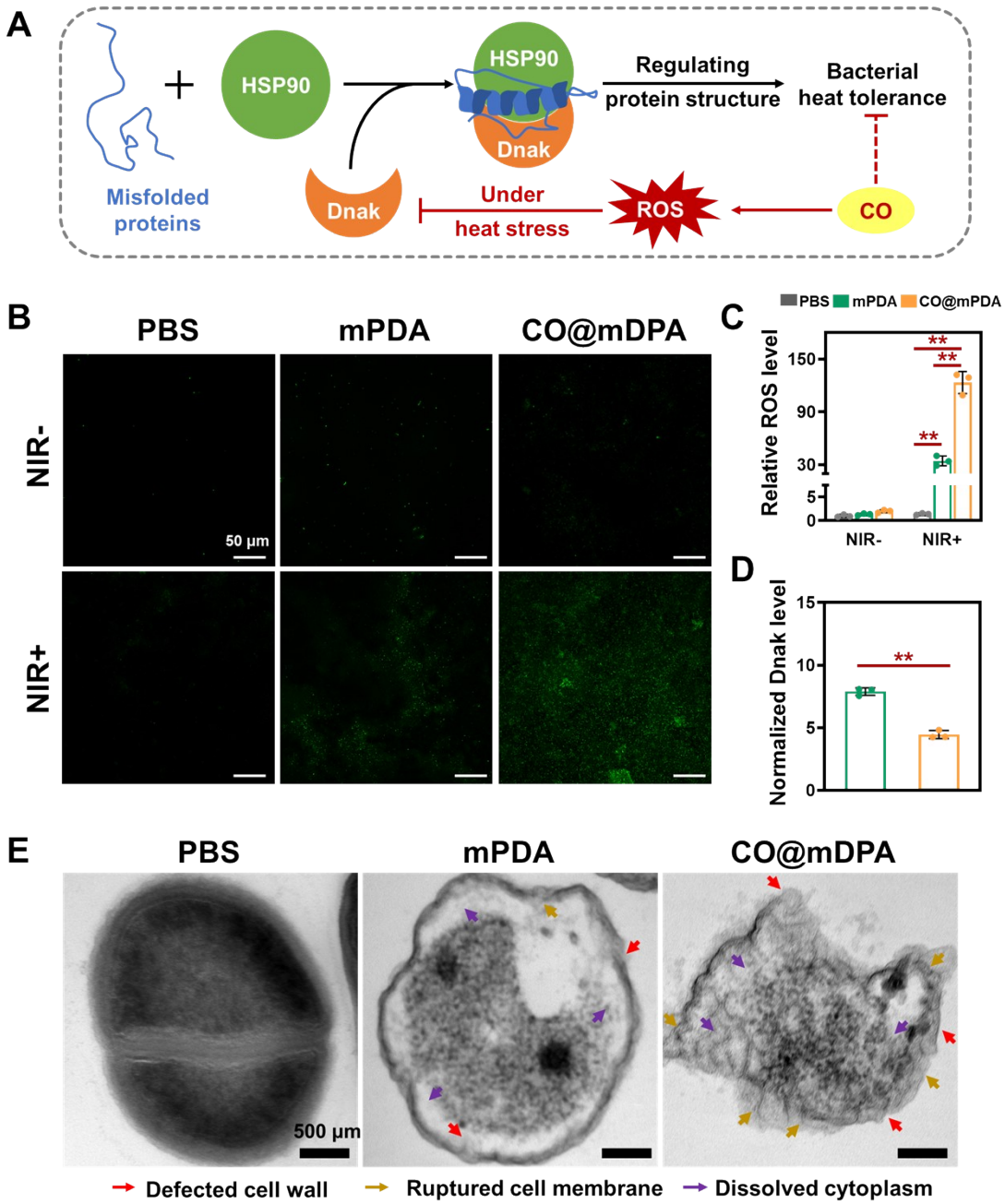

Fig. S7. Verification of the possible antibacterial mechanism of CO-mediated PTT.

(A) Schematic illustration of possible antibacterial mechanism. (B-C) The representative images of DCFH-DA fluorescent staining (B) and quantitative result of relative fluorescence intensity (C). (D) Dnak gene expression in bacteria after various treatments. (E) The representative TEM images of bacteria after various treatments. All data are shown as mean ± s.d. (n = 3). The differences were determined by student's t-test between two groups and one-way ANOVA for three groups. The significance was marked as '**' for $P < 0.01$, '*' for $P < 0.05$ and 'ns' for $P > 0.05$.

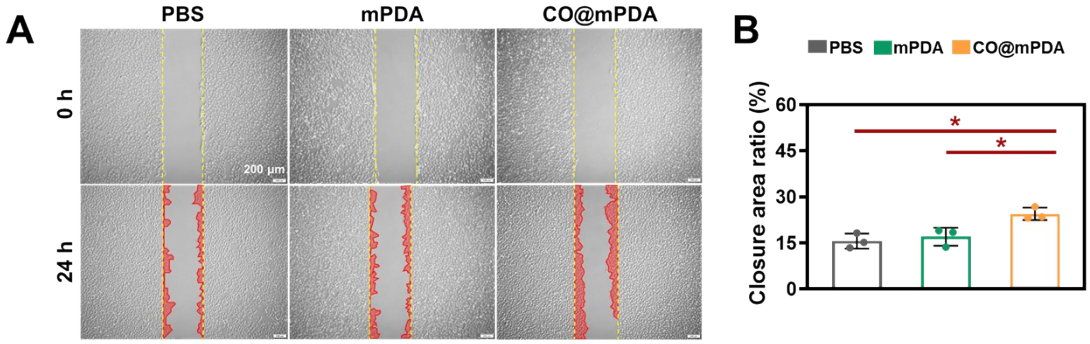

Fig. S8. The migration of HUVECs at 24 hours after various treatment.

The representative images of scratch assays (A) and its statistical analysis (B). All data are shown as mean ± s.d. (n = 3). The differences were determined by one-way ANOVA for three groups. The significance was marked as '**' for $P < 0.01$, '*' for $P < 0.05$ and 'ns' for $P > 0.05$.

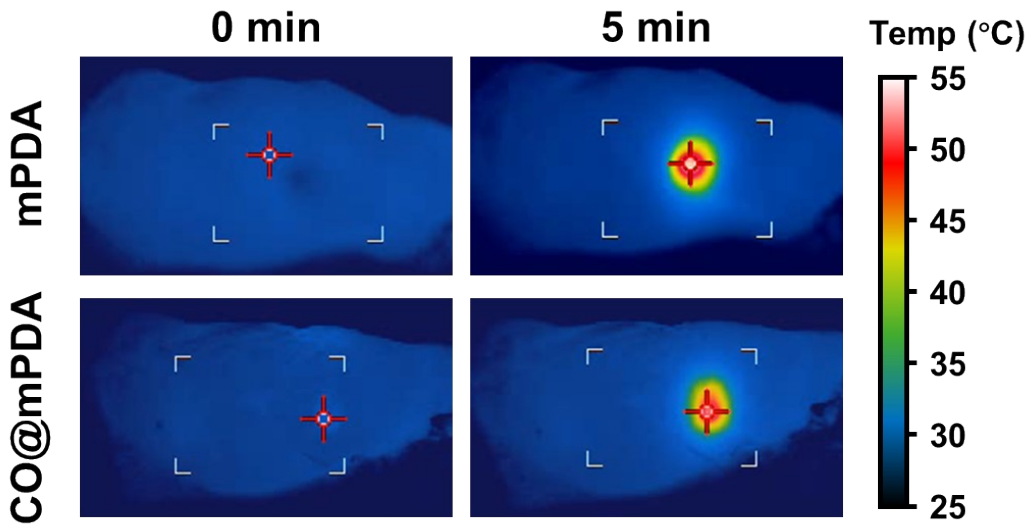

Fig. S9. *In-vivo* photothermal conversion performance of CO@mPDA.
Representative *in-vivo* IR images after being irradiated for pre-set period.

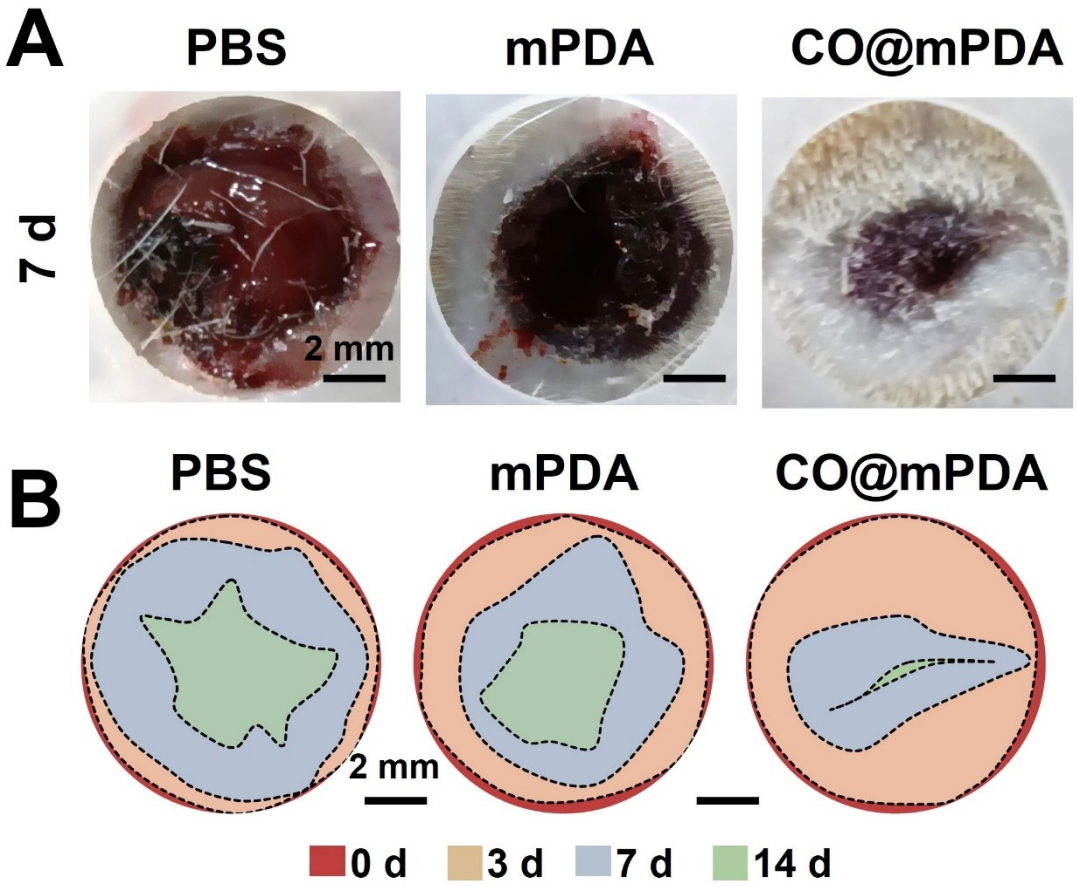

Fig. S10. Representative general views of wound beds.

(A) Representative general views at day 7 post various treatments. (B) The changes of wound shapes during the treatment.

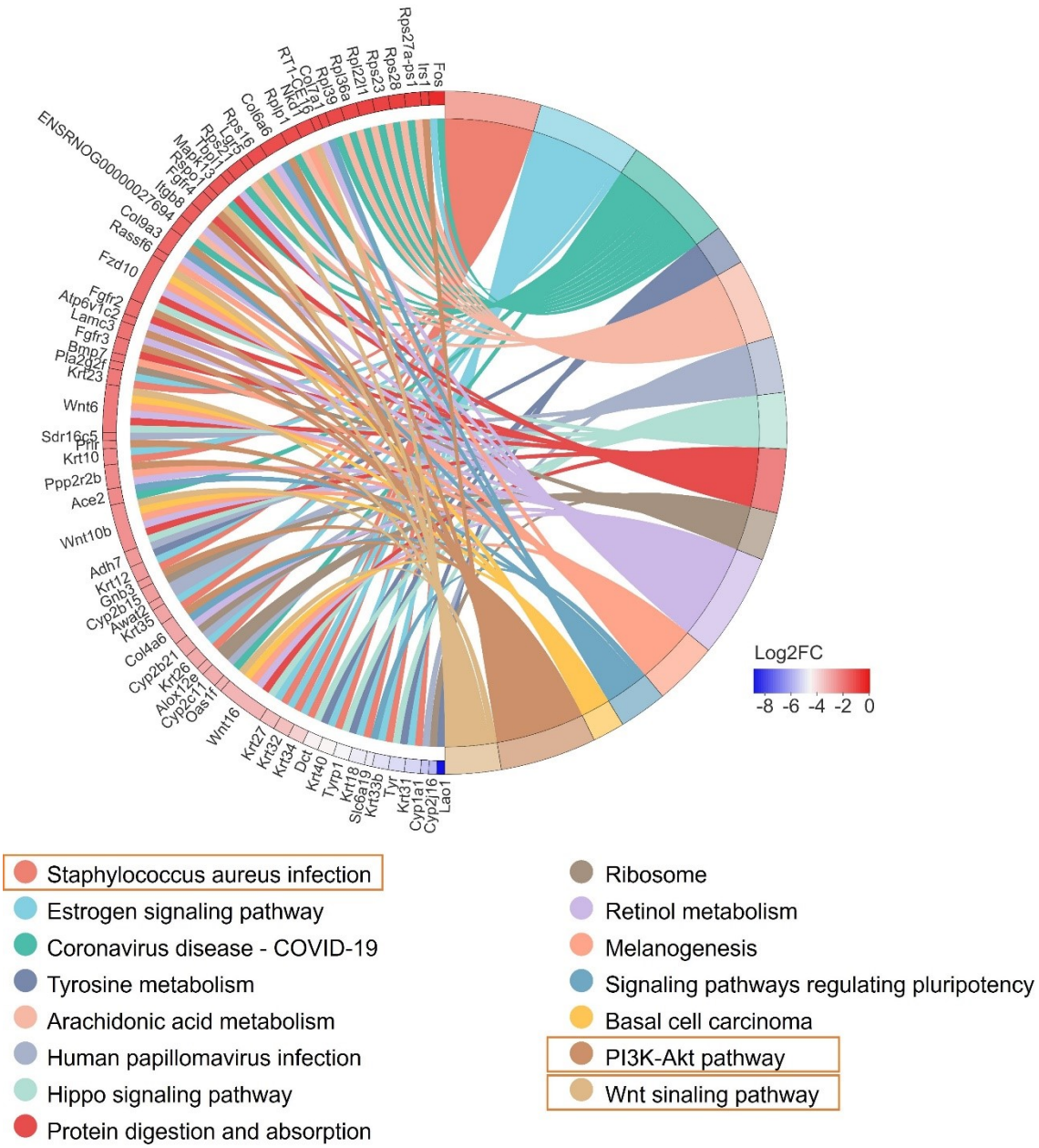

Fig. S11. Fan chart of KEGG analysis of enriched pathways between mPDA and CO@mPDA treatment.

Yellow frame marked the noteworthy KEGG terms.

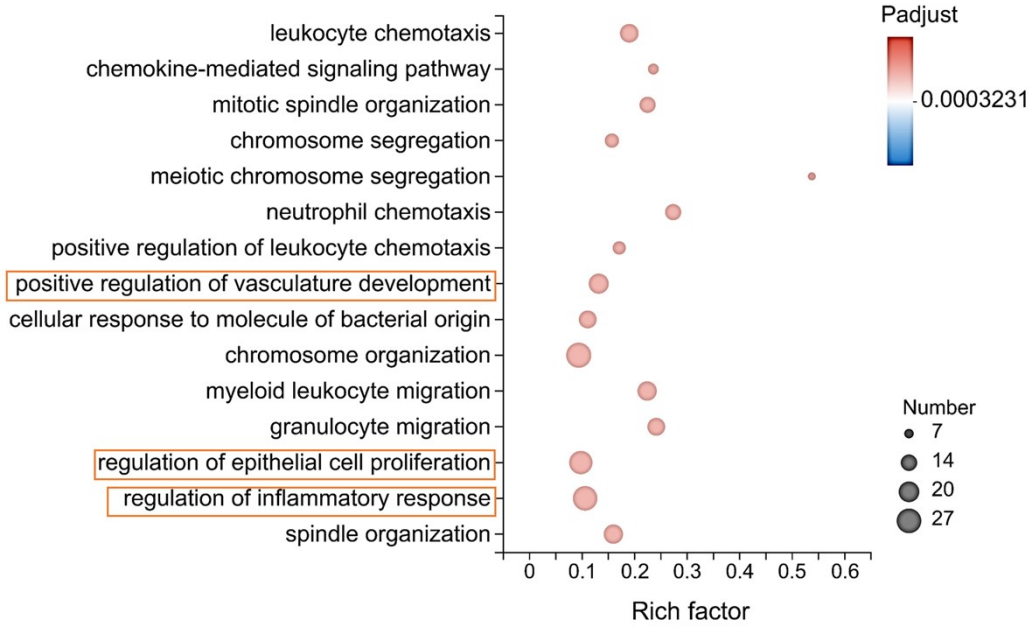

Fig. S12. GO analysis between mPDA and CO@mPDA treatment.

Yellow frame marked the noteworthy GO terms.

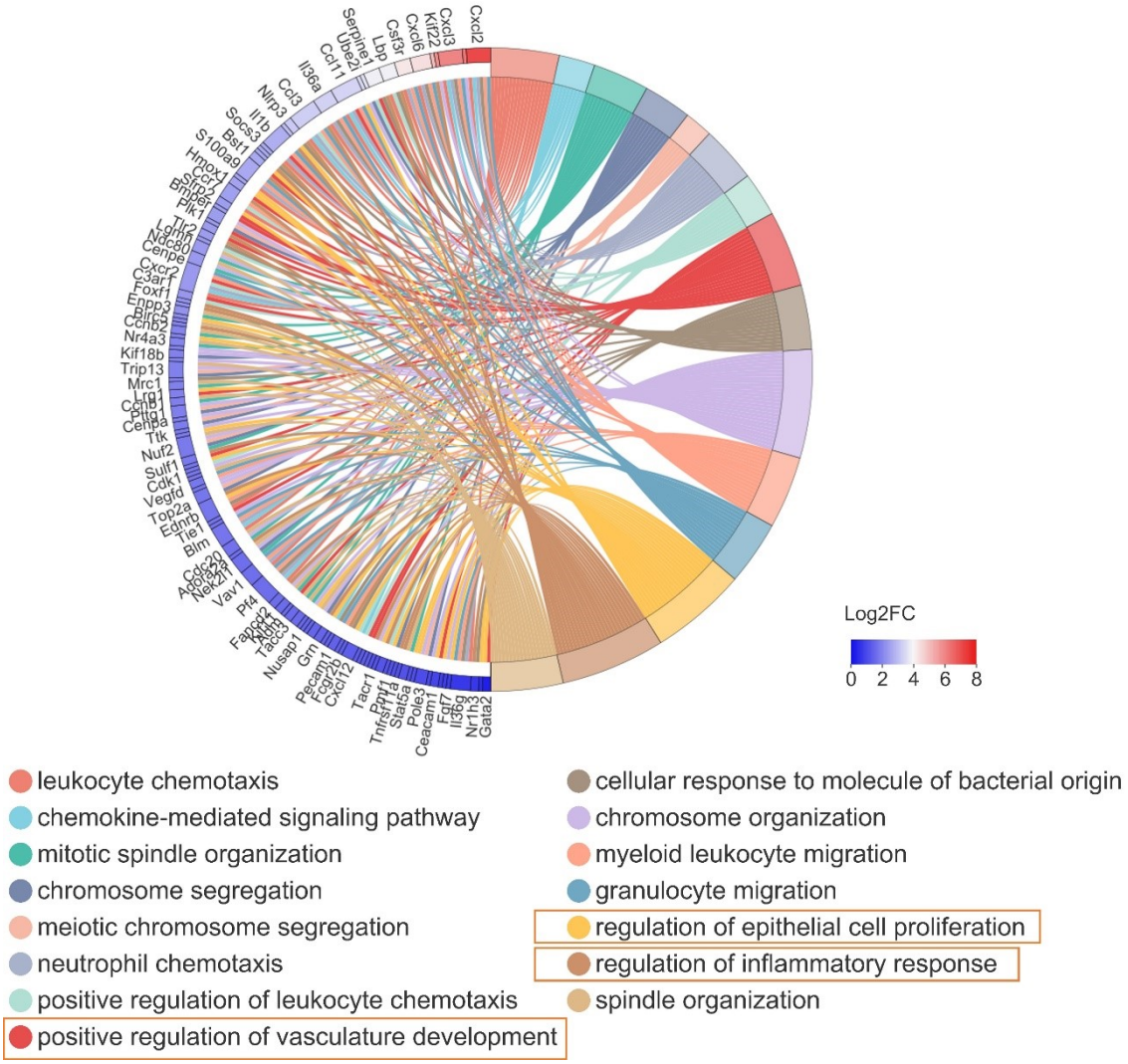

Fig. S13. Fan chart of GO analysis between mPDA and CO@mPDA treatment.

Yellow frame marked the noteworthy GO terms.

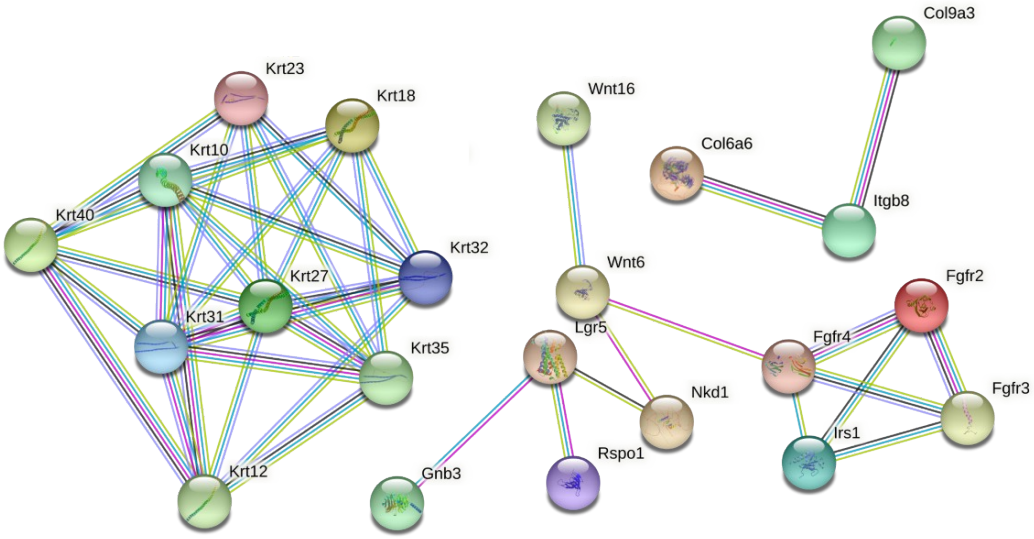

Fig. S14. PPI network of DEGs involved in pathophysiological features of infected diabetic wound by CO-mediated PTT.

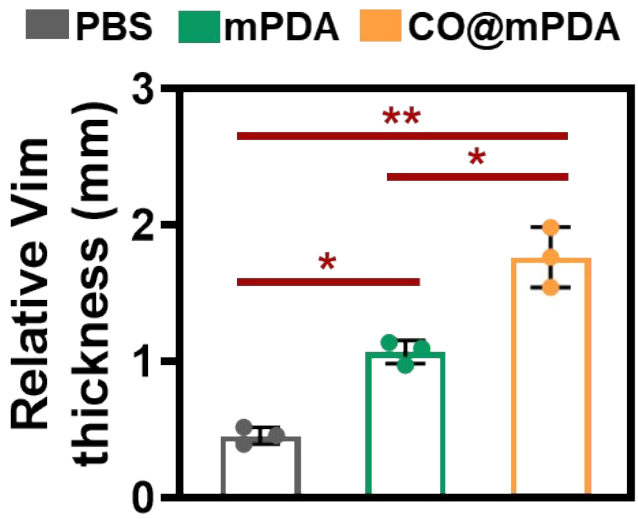

Fig. S15. Statistical results of Vim thickness on day 14 post CO-mediated PTT.

All data are shown as mean ± s.d. (n = 3). The differences were determined by one-way ANOVA. The significance was marked as '**' for $P < 0.01$, '*' for $P < 0.05$, and 'ns' for $P > 0.05$.

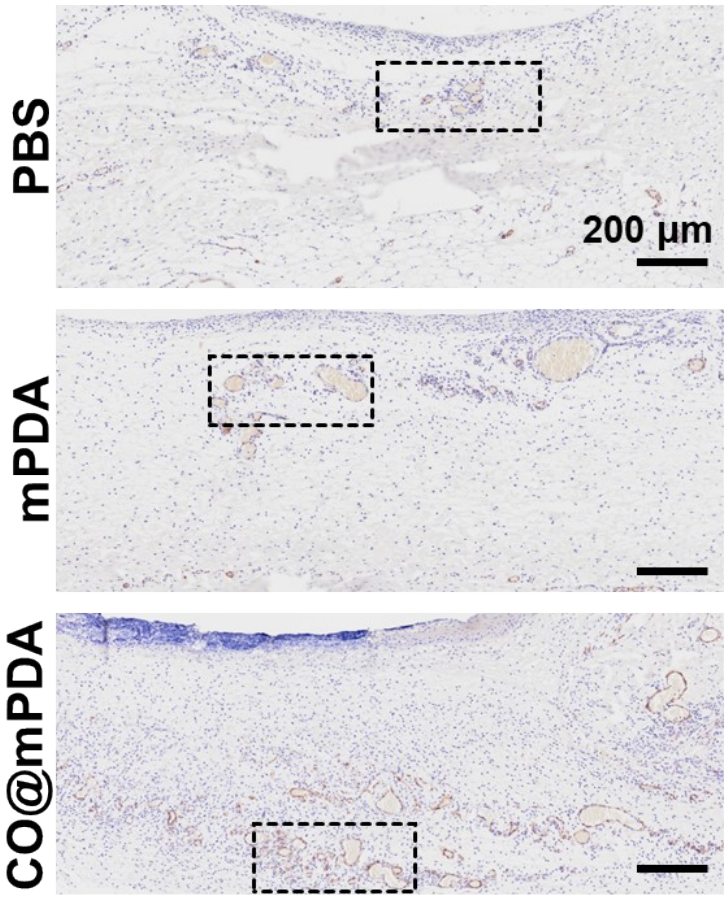

Fig. S16. Representative images of immunohistochemistry staining of CD31 on day 14 post CO-mediated PTT.

The black frame indicated the zoom-up zones that displayed in Fig. 6H.

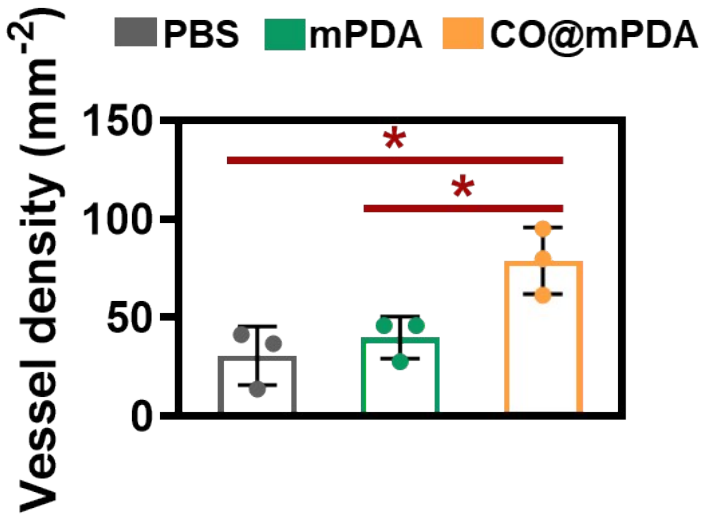

Fig. S17. Statistical results of Vessel density on day 14 post CO-mediated PTT.

All data are shown as mean ± s.d. (n = 3). The differences were determined by one-way ANOVA. The significance was marked as '**' for $P < 0.01$, '*' for $P < 0.05$, and 'ns' for $P > 0.05$.

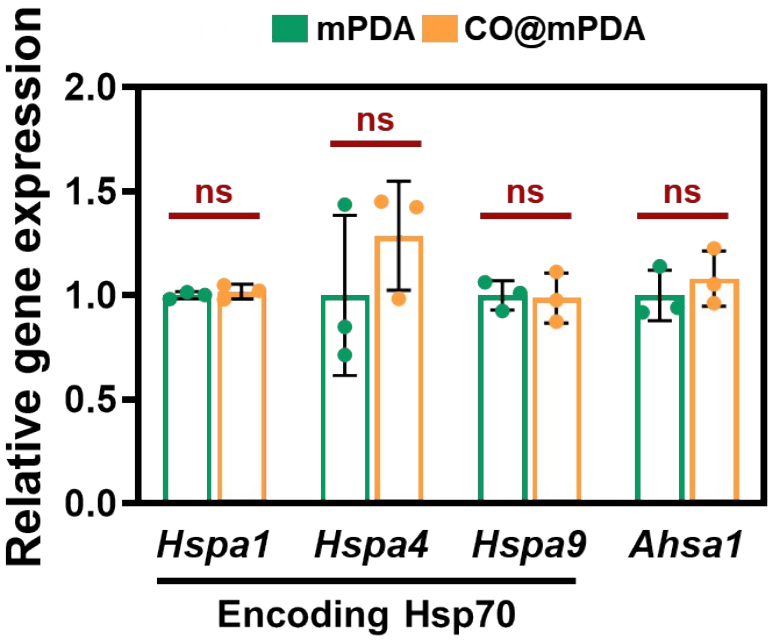

Fig. S18. The relative gene expression of Hsp70 and Ahsa1in tissues after various treatments.
All data are shown as mean ± s.d. (n = 3). The differences were determined by one-way ANOVA. The significance was marked as '**' for P < 0.01, '*' for P < 0.05, and 'ns' for P > 0.05.

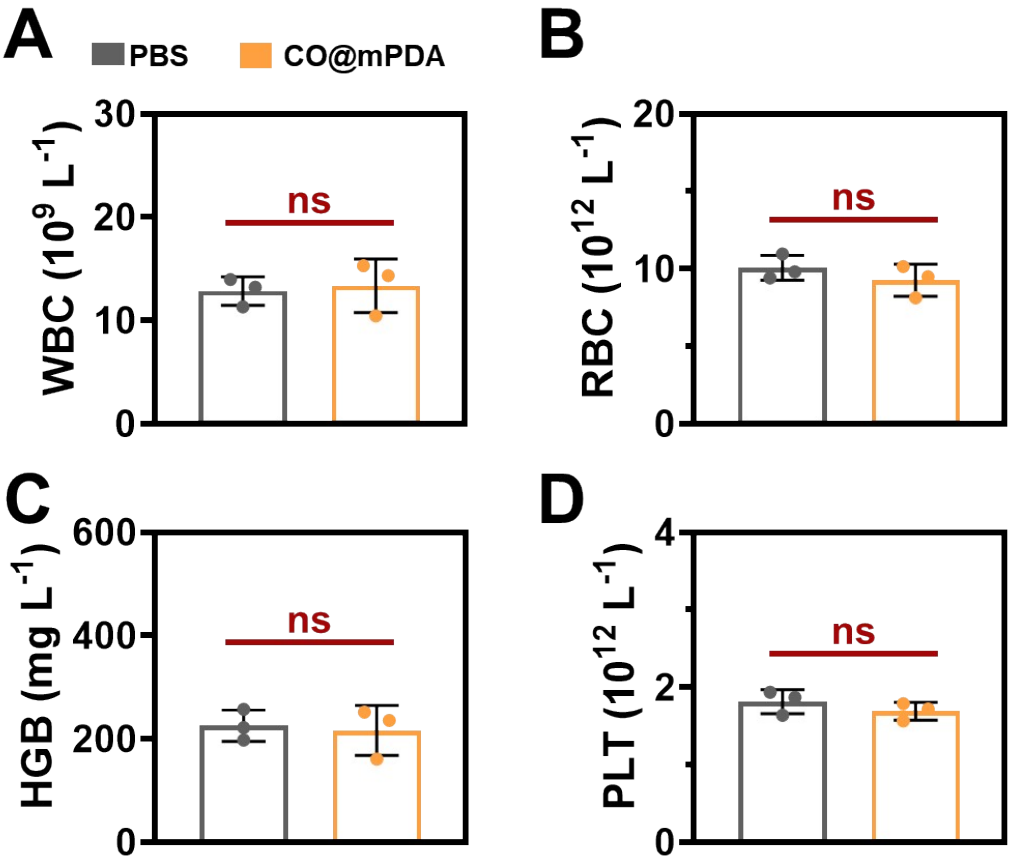

Fig. S19. Routine blood test after CO-mediated PTT on day 14 post CO-mediated PTT.
Blood parameters on day 14 post CO-mediated PTT, including the level of RBC (A), WBC (B), HGB (C), PLT (D). All data are shown as mean ± s.d. (n = 3). The differences were determined by student *t*-test. The significance was marked as '**' for $P < 0.01$, '*' for $P < 0.05$, and 'ns' for $P > 0.05$.

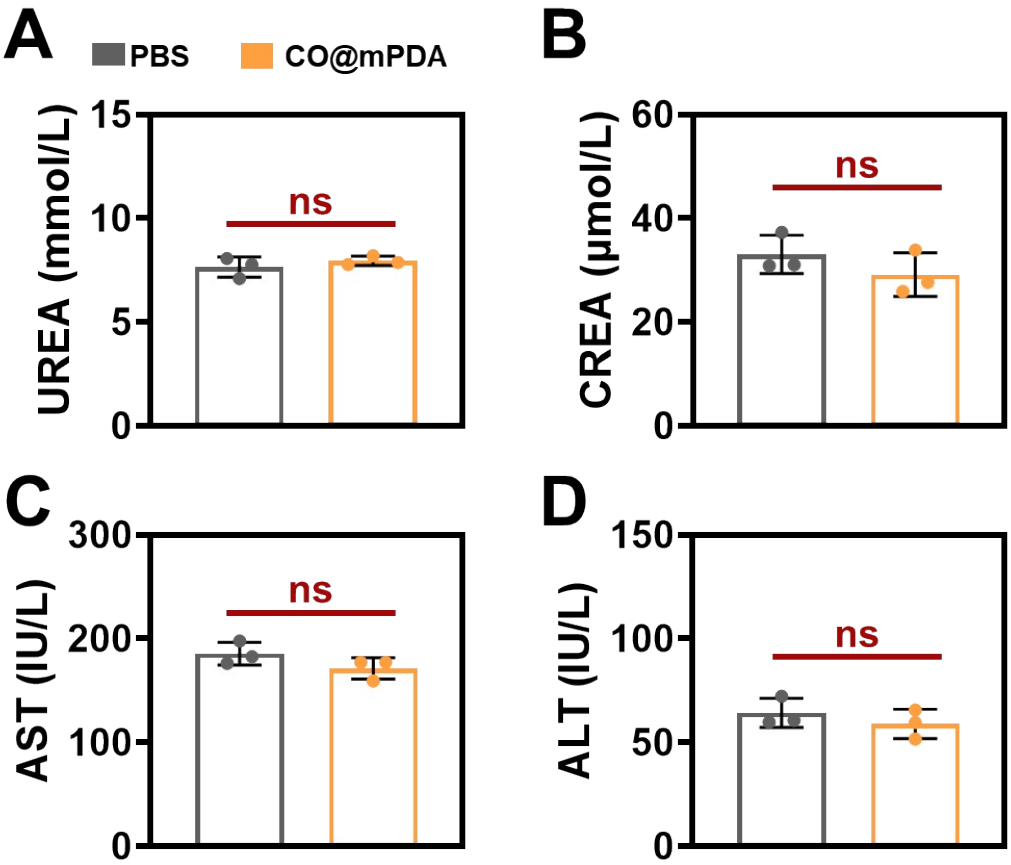

Fig. S20. Evaluation of liver and kidney function after CO-mediated PTT.

Blood parameters on day 14 post CO-mediated PTT, including the level of Urea (A), CREA (B), AST (C) and ALT (D). All data are shown as mean ± s.d. (n = 3). The significant difference was marked as '**' for $P < 0.01$, '*' for $P < 0.05$, and 'ns' for $P > 0.05$.

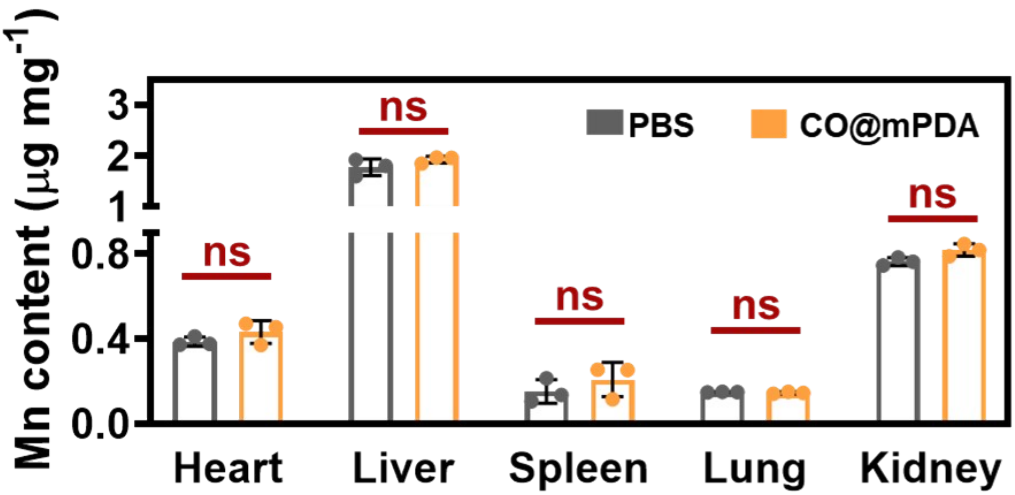

Fig. S21. Mn content in the major organs on day 14 post CO-mediated PTT.

Mn concentration in the heart, liver, spleen, lung, and kidney tissues of SD rat after various treatment. All data are shown as mean ± s.d. (n = 3). The differences were determined by student's t-test between two groups. The significant difference was marked as '**' for $P < 0.01$, '*' for $P < 0.05$, and 'ns' for $P > 0.05$.

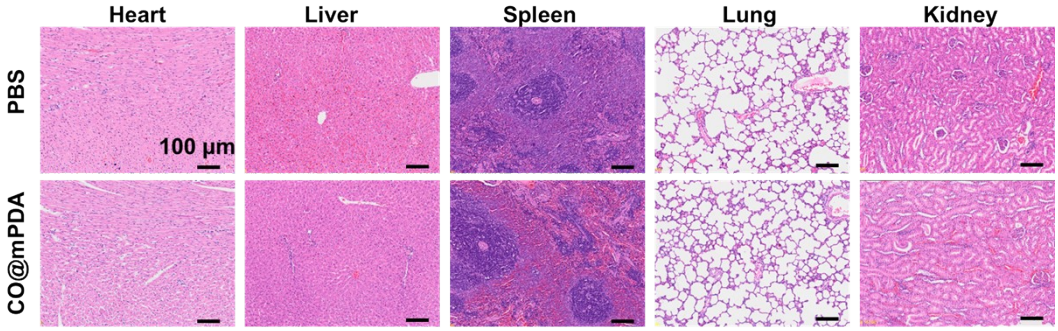

Fig. S22. Representative histological images of major organs on day 14 post CO-mediated PTT.